RESEARCH ARTICLE

annalen der physik
www.ann-phys.org

Hybrid Orbital Formation and Multicenter Bonding of Hydrogen Atoms and Molecules in Ti_3C_2 MXenes

Norbert H. Nickel

The formation and stability of solids and molecules is not possible without chemical bonds, which are divided into covalent, ionic, metallic, and van der Waals bonds. A special type of intermolecular bond is hydrogen bonding, which plays a crucial role for chemical, biological, and physical processes. However, hydrogen shows a far more complex behavior when it is present in solids. In this paper, it is shown that the chemical bonding of hydrogen atoms and molecules extends far beyond the simple picture of conventional, ionic, covalent, and multicenter bonds. The interaction of H with its host material is particularly important for hydrogen storage in metallic materials such as Ti_3C_2 MXenes. Hydrogen atoms and H_2 molecules form multicenter bonds in Ti_3C_2. On the surface and between two Ti_3C_2 sheets this is limited to the formation of H–Ti bonds. However, H and H_2 on interstitial sites form multicenter bonds not only with nearest neighbor Ti atoms but also with carbon atoms. Interestingly, the H–C bonds are characterized by the formation of s–p hybrid orbitals. For H_2 molecules, multicenter bond formation is accompanied by an increase of the bond length to 2.07 and 1.85 Å for H_2 on the surface and at the interstitial site, respectively. On the other hand, placing H_2 between two sheets of Ti_3C_2 leads to dissociation. For all H and H_2 complexes the vibrational eigenmodes are calculated. Their frequencies are in the range of 890 to 1610 cm^{-1}, which indicates that the bonds are remarkably strong.

1. Introduction

Chemical bonds enable the formation of molecules and solids due to the attraction of valence electrons of atoms. The simple representation of a covalent bond depicts a pair of electrons that is occupying the space between the two atoms. In ionic bonds the electrons are not equally distributed between atoms but attracted to the more electronegative atom. In metals the bonding mechanism is different. Each atom of the solid gives up its valence electrons, which then form a quasi-free electron gas. Bonding occurs because of an attractive force between the positively charged atoms and the quasi-free electron gas. In addition, there are types of weak bonds such as Van der Waals bonds and hydrogen bonding that rely on dipole–dipole forces.

Compared to these bonding modes, hydrogen shows a far more complex behavior. For example, in p-type crystalline silicon, H atoms can occupy a bond-center site between two Si atoms. In this case, the charge of the H atom is donated to the conduction band and the H complex acts as a donor.[1,2] In molecules H can also form 3-center bonds. An example is B_2H_6 where each boron atom is tetrahedrally surrounded by four H atoms.[3] The bonding behavior of H becomes even more interesting when hydrogen is present in wide bandgap oxides. When hydrogen substitutes oxygen atoms it forms uniform bonds to all nearest neighboring metal atoms. Hence, in zinc oxide and magnesium oxide substitutional H becomes fourfold and sixfold coordinated, respectively.[4]

In this paper, it is shown that the chemical bonding of hydrogen with other elements is more complex than has been thought previously. Bonding extends far beyond the simple picture of conventional, ionic, covalent, and multicenter bonds. The formation of multicenter H bonds is a property characterized by the presence of metal atoms and their ability to interact with the s-orbital of hydrogen atoms. However, the formation of multicenter bonds is not limited to isolated H atoms. Here it is shown that even molecular H_2 forms stable multicenter bonds.

The structural and electronic properties of H were investigated for Ti_3C_2, which belongs to a class of 2D materials known as MXenes. These 2D materials are composed of early transition metals, M_{n+1}, that alternately bind to n layers of carbon or nitrogen. Hence, the basic formula is given as $M_{n+1}X_nT_y$, where X is replaced by C or N and the last term denotes a possible surface termination.[5]

MXenes combine properties of metals and ceramics.[6] They exhibit excellent mechanical strength, high thermal conductivity, and the bandgap can be tuned from metallic to semiconducting.[5,7,8] The variety of properties and the combination of different MXenes open up the way for a multitude of potential applications. For example, MXenes can be used to harvest energy in the form of solar energy, thermoelectric energy, piezoelectric energy, and more.[9] Due to their chemical and structural

N. H. Nickel
Helmholtz-Zentrum Berlin für Materialien und Energie GmbH
Nanoscale Solid-Liquid Interfaces
Schwarzschildstr. 8, 12489 Berlin, Germany
E-mail: nickel@helmholtz-berlin.de

The ORCID identification number(s) for the author(s) of this article can be found under https://doi.org/10.1002/andp.202400011

DOI: 10.1002/andp.202400011

diversity, some MXene layers are suitable for energy storage in batteries or super capacitors.[10] Recently, the use of MXenes in biomedicine opened up one of the most exciting areas of research spanning topics such as dialysis, photothermal cancer therapy, and neural electrodes.[11,12]

For future energy security, photo and electro catalysis will play an important role. In particular, hydrogen evolution reactions are of increasing interest, since H is considered as an energy alternative due to its high calorific value. MXenes also score in this area with their exceptional electronic, structural, and chemical properties. An overview of the performance of several MXenes as electrocatalysts for the hydrogen evolution reaction can be found in ref. [13]. An interesting new application of MXenes is the idea of using them for hydrogen storage.[14] In fact, the presence of H_2 in Ti_3C_2 MXenes was confirmed using neutron scattering experiments.[15] Moreover, Molecular dynamic simulations indicate that 3.4 wt% H_2 can be adsorbed and released under ambient conditions.[16] In this context, an important question arises regarding the nature of the interaction and bonding of hydrogen with MXenes.

The exposure of MXenes to hydrogen is not limited to hydrogen storage. Many applications of MXenes are based on the interactions of devices and sensors with chemicals that can lead to the generation of hydrogen atoms and molecules. Besides hydrogen storage, this also applies to photo- and electrocatalysis.

Once H atoms or molecules are present, there is a high probability that they will interact with solids. In semiconductors and metals the properties of hydrogen have been extensively investigated. Hydrogen is known to adsorb on surfaces, passivating dangling bonds, migrate into solids where it can neutralize doping atoms and dangling bonds, and even create new structural and electronically active defects.[17–19]

Here it is shown that the formation of hydrogen multicenter bonds also occurs in metallic materials such as Ti_3C_2 MXenes. Furthermore, multicenter bond formation also occurs for H_2 molecules in Ti_3C_2 MXenes, which is accompanied by a significant increase of the H–H bond distance. In addition to the formation of metal–H bonds, monatomic and molecular hydrogen accommodated at interstitial sites form further bonds to nearest neighbor carbon atoms. These bonds are characterized by the formation of s–p hybrid orbitals. Calculations of the vibrational eigenmodes shows that resulting multicenter H and H_2 complexes are stable.

The interaction of H and H_2 with MXenes can affect the physical and chemical properties of its host. This can manifest itself in changes in the crystal structure and influence mechanical properties such as hardness and elasticity, as well as chemical stability. The latter could, for example, manifest itself as a degradation effect in hydrogen storage applications. Therefore, understanding of the chemical bonding of hydrogen in MXenes is of great interest.

2. First-Principles Calculations

The results presented in this section were obtained by placing H atoms and H_2 molecules on top, inside, and between sheets of Ti_3C_2. For monatomic H and molecular H_2 the equilibrium structures and corresponding density-of-states distributions are described in Sections 2.1 and 2.2, respectively. Section 2.3 is focused on the vibrational eigenmodes of the multicenter H complexes.

2.1. Monatomic Hydrogen

Ti_3C_2 belongs to the hexagonal space group P6 3/mmc and forms a 2D sheet-like structure. Since the surfaces of these sheets are terminated with Ti atoms they are susceptible to oxidation. On the other hand, hydrogen is one of the most well-known elements for passivating surfaces and has been used effectively to passivate surfaces of semiconductors such as silicon and germanium.[20,21] When H is placed on top of Ti_3C_2 its lowest energy site is in a hexagonal center of the surface with three surface Ti atoms as nearest neighbors (see **Figure 1a**). In addition, the electronic charge density distribution of the H ad-atom is shown in Figure 1a in a top and edge-on view. The data clearly show that the H ad-atom binds to the three nearest neighbor Ti atoms. Hence, the H atom exhibits a threefold coordination despite the fact that H has an electronic structure of $1s^1$ and is widely believed that it forms only one single chemical bond. The bond length of the three Ti–H bonds amounts to 2.04 Å, which is only slightly shorter than the Ti–C bond length of 2.08 Å.

The nature of the hydrogen chemical bond was further investigated by analyzing the density-of-states (DOS). In Figure 1b the total DOS of Ti_3C_2 with and without an adsorbed H atom is shown by the black and red curves, respectively. Comparing the two curves reveals a shoulder in the DOS at $E = -5.5$ eV for H adsorbed on the surface of Ti_3C_2 (see arrow in Figure 1b). The projection of the DOS on the H atom and the three nearest neighbor Ti atoms shows that the shoulder originates from a superposition of the s-orbitals of the H and Ti atoms (see Figure 1c). Second nearest and further distant neighbor Ti atoms do not contribute to the peak located at $E = -5.5$ eV. Hence, this clearly shows that H atoms form multicenter bonds on the surface of Ti_3C_2. The character of the multicenter H bonds can be classified as covalent within the density-functional theory (DFT) model approximation, excluding Van der Waals interaction.

A further position that can accommodate H atoms is the interstitial site in the center of Ti_3C_2. The complex is depicted in **Figure 2a** in a top and edge-on view. In addition, the electronic charge density distribution is shown. The interstitial H atom forms bonds to three nearest neighbor Ti atoms and to the nearest neighbor C atom, which is located directly below the interstitial site. All three Ti–H bonds have a bond length of 1.88 Å, which indicates that the interstitial site is highly symmetrical. The fourth bond of the H atom extends to the nearest C atom with a bond length of 1.22 Å. This is ≈ 7% longer than the C–H bond length on a diamond surface.[22]

The total and local DOS projected on the H, Ti, and C atoms are shown in Figures 2b and 2c, respectively. In the total DOS two peaks emerge that are located at $E = -6.77$ eV and $E = -12.99$ eV. Both peaks originate from a projection of the density-of-states on the H atom and its nearest neighbor Ti and C atoms. For interstitial H an hitherto unexpected behavior is observed. The s-orbitals of the involved atoms split and the superposition of the s-orbitals of the H, Ti, and C atoms occurs at $E = -6.77$ eV and $E = -12.99$ eV. This split of 6.22 eV is too large to be caused by a state or symmetry breaking degeneracy. A closer look into the s- and p-orbitals

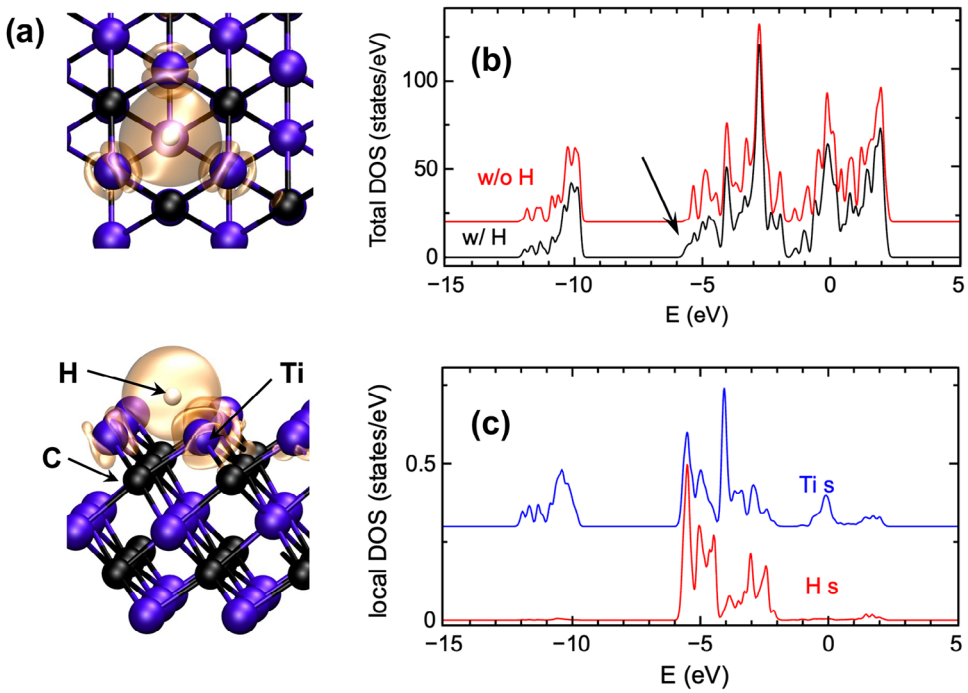

Figure 1. Depiction of the equilibrium position of atomic H on top a) of a Ti_3C_2 layer. The depicted iso-surface corresponds to the lowest energy bonding state of the hydrogen atom. The cutoff amounts to 8×10^{-3} eV Å^{-3}. b) The total density-of-states (DOS) for a pristine Ti_3C_2 (red curve; w/o H) and an adsorbed H atom on the surface (black curve; w/ H). c) Shows the projected DOS of the H atom and its nearest neighbor Ti atoms. Note that the spectra for the total and local DOS are shifted vertically for clarity. The Ti, C, and H atoms are depicted by purple, black, and white spheres, respectively.

provides insight into the origin of the two states associated with interstitial H. In Figure 2d the projected DOS of the s-orbitals of C and H and the projected DOS of the p-orbitals of C are shown. While the p_x and p_y orbitals do not contribute to the observed peaks in the local DOS, the carbon p_z orbital exhibits a significant contribution to both peaks. For comparison, in pristine Ti_3C_2 the two peaks are not observed in the local DOS (see Figure 2e). Thus, this result clearly establishes that the s-orbital of interstitial H forms a hybrid orbital with the p_z-orbital of the adjacent C atom.

A third stable position for H atoms is located between two Ti_3C_2 sheets (**Figure 3a**). The H atom forms three bonds to surface Ti atoms of the lower Ti_3C_2 sheet with Ti–H bond lengths of 1.96, 1.96, and 2.02 Å. This is similar to H on the surface of Ti_3C_2 (see Figure 1a). In addition, a fourth bond with a bond length of 1.91 Å is formed with a surface Ti atom of the second Ti_3C_2 sheet. The formation of chemical bonds between the H atom and 4 surrounding Ti atoms is further supported by the DOS. The total density-of-states (Figure 3b) exhibits an additional peak at $E = -6.3$ eV that is attributed to a superposition of the s-orbitals of the H atom and its four nearest neighbor Ti atoms (see Figure 3c).

2.2. Molecular Hydrogen-

The most stable configuration of hydrogen are molecules. Their electronic configuration is $1s^2$ and the dissociation energy amounts to 4.516 eV,[23] which renders H_2 inert under ambient conditions. However, the reactivity of molecular hydrogen changes significantly as the molecules approach Ti_3C_2. When H_2 reaches the surface the molecule forms six chemical bonds with 4 Ti atoms (see **Figure 4a**). The bond length of the H_2 molecule increases from 0.75 to 2.07 Å. The Ti–H bond lengths vary between 1.95 Å for the Ti–H bonds in [1$\bar{2}$10] direction to 2.02 and 2.14 Å for the remaining four Ti–H bonds. The Ti–H bonds give rise to an additional peak in the total DOS located at $E = -5.95$ eV (Figure 4b). The local DOS projected on the H and Ti atoms shows that the additional peak is a due to a superposition of the s-orbitals of the H and Ti atoms (Figure 4c).

Within a Ti_3C_2 sheet stable positions for H_2 molecules are interstitial sites. The configuration is similar to that for monatomic H. However, the H–H bond length increases from 0.75 to 1.85 Å, since both H atoms reside exactly above or below a C atom with which they form chemical bonds (see **Figure 5a**). The bond length of both C–H bonds amounts to 1.22 Å and is thus the same as for monatomic H at the interstitial site (see Figure 2). In addition, both H atoms form chemical bonds to the nearest neighbor Ti atoms. This is similar to the configuration of H_2 on the surface of Ti_3C_2 (see Figure 4).

For interstitial H_2 the density-of-states shows a uniqueness compared to the DOS of interstitial H. Similar to interstitial H (Figure 2), there are two additional peaks in the DOS. However, for molecular hydrogen both additional peaks split into two peaks each. The local DOS projected on the H, Ti, and C atoms reveals that the origin of the peaks located at $E_1 = -13.69$ eV and $E_2 = -12.50$ eV originate from a superposition of the s-orbitals of the H, Ti, and C atoms, while the two peaks located at $E_3 = -7.11$ eV and $E_4 = -6.67$ eV are caused by a superposition of the H s-orbitals and the C p_z-orbitals (Figure 5c). Note that the p_x and p_y orbitals do not contribute to the additional peaks in the DOS.

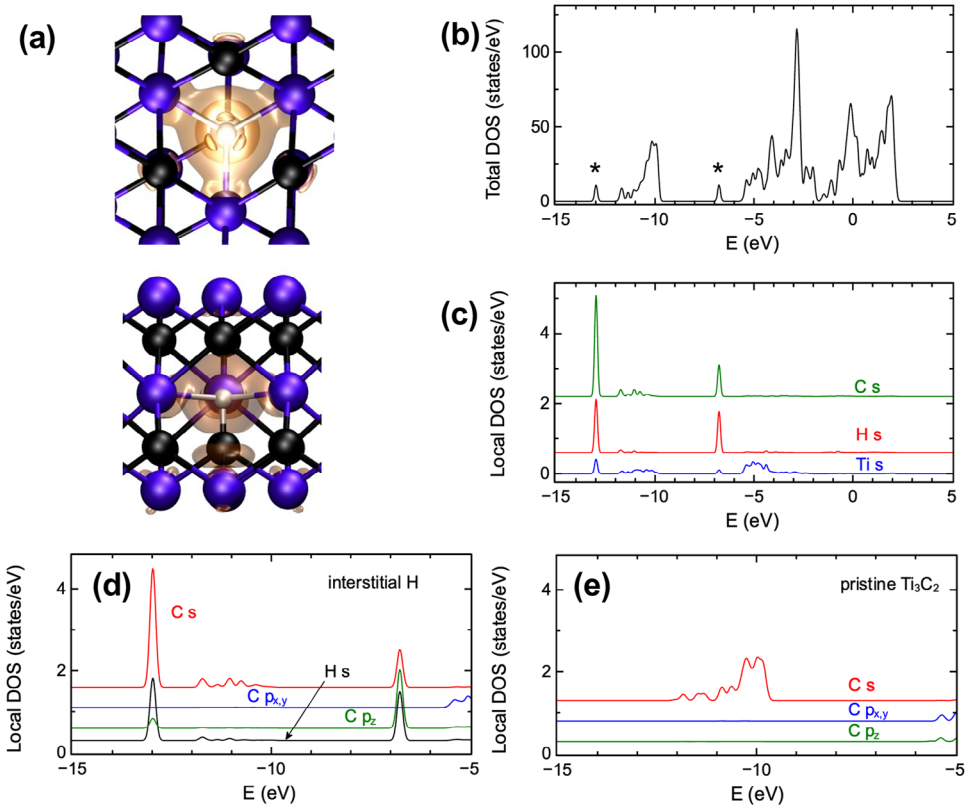

Figure 2. a) Depiction of atomic H in the interstitial site in the center of Ti_3C_2. Also shown is the iso-surface that corresponds to the lowest energy bonding state of the H atom. The cutoff amounts to 8×10^{-3} eV Å^{-3}. The total DOS is plotted in b). The asterisks mark the new peaks due to the presence of the H atom. The projected DOS of the s-orbitals of the H atom and its nearest neighbor Ti and C atoms are shown in c). In addition, the projected DOS of the carbon p-orbitals is shown for d) interstitial H and e) for H-free Ti_3C_2. Note that the spectra are shifted vertically for clarity.

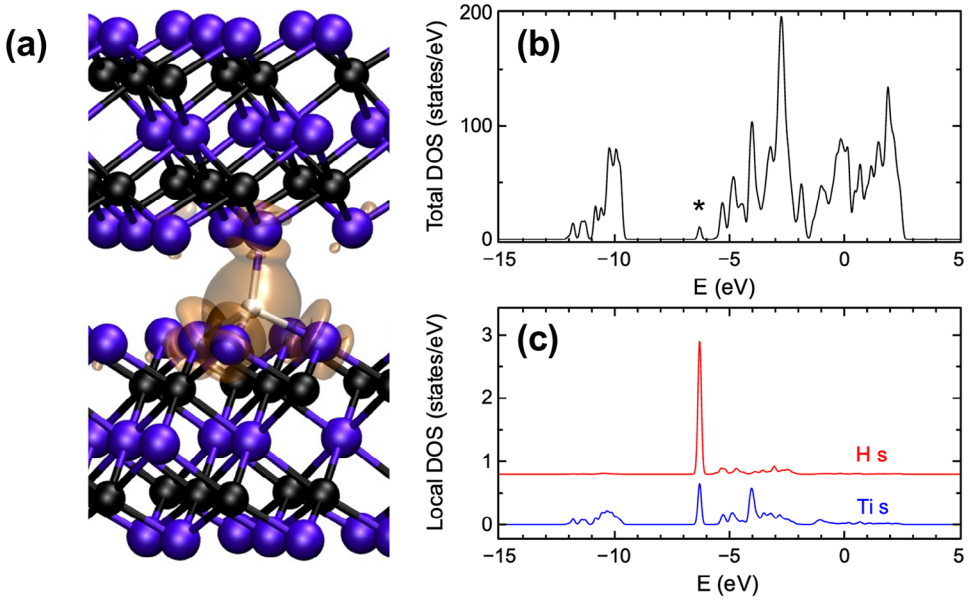

Figure 3. a) Depiction of atomic H between two layers of Ti_3C_2. The iso-surface shown for a cutoff of 8×10^{-3} eV Å^{-3} corresponds to the lowest energy bonding state of the H atom. b) Shows the total DOS. The asterisk marks the new peak due to the presence of the H atom. c) Shows the projected DOS of the s-orbitals of the H atom and its nearest neighbor Ti atoms. Note that the spectra are shifted vertically for clarity.

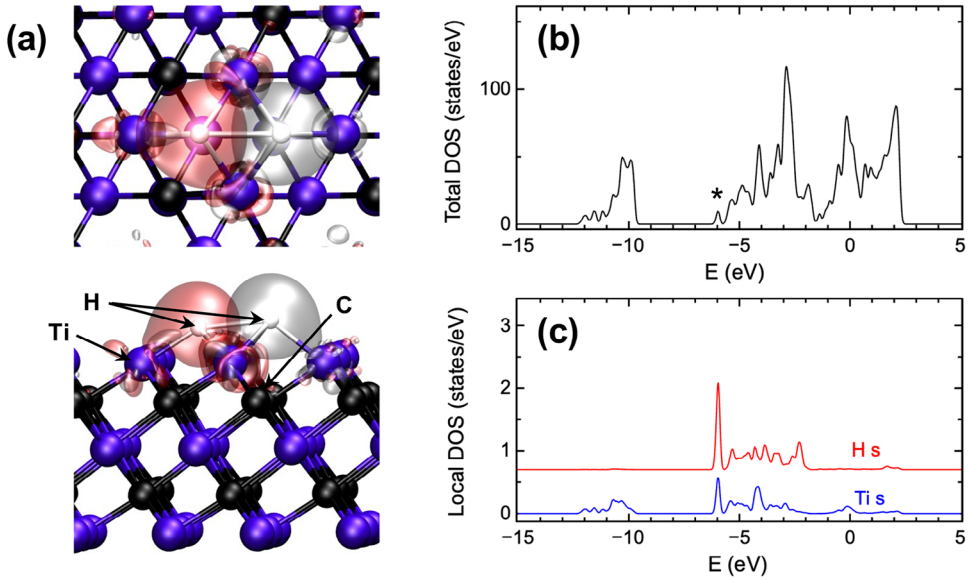

Figure 4. a) Depiction of the equilibrium positions of molecular hydrogen (H_2) on top of a Ti_3C_2 layer in a surface and edge-on projection. The depicted iso-surfaces correspond to the lowest energy bonding state of the hydrogen atoms. In order to better distinguish between the two atoms, their iso-surfaces are shown in different colors. The cutoff amounts to $8{\times}10^{-3}$ eV Å^{-3}. b) Shows the total density-of-states (DOS). The asterisk marks the new peak due to the presence of the H molecule. c) Shows the projected DOS of the H_2 molecule and its nearest neighbor Ti atoms.

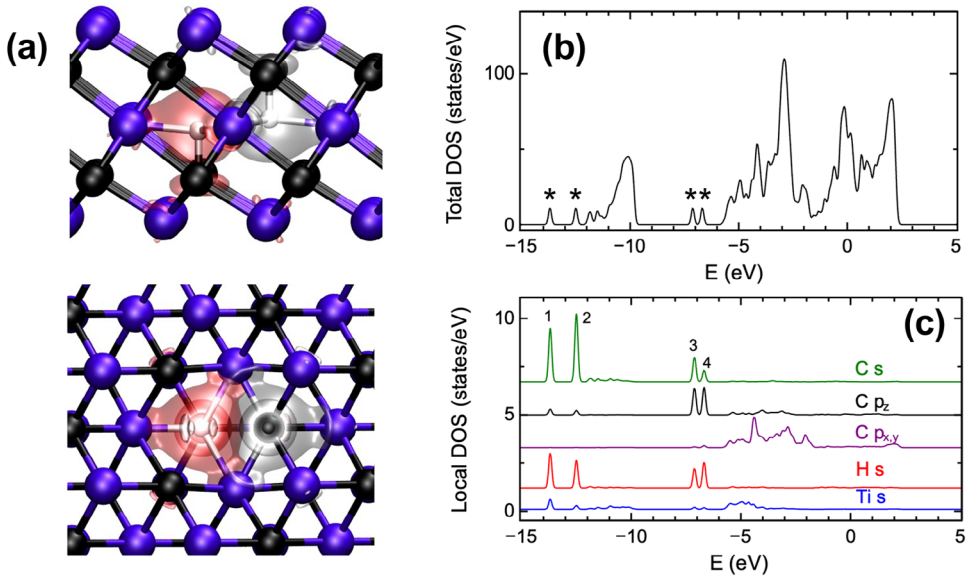

Figure 5. Depiction of the equilibrium positions of molecular hydrogen (H_2) in a Ti_3C_2 layer. Shown are an edge-on and top view projection a) including iso-surfaces corresponding to the lowest energy bonding state of the hydrogen molecule. To better distinguish between the two atoms, the iso-surfaces are shown in different colors. The cutoff amounts to 8×10^{-3} eV Å^{-3}. b) Shows the total density-of-states (DOS). The asterisks mark the new peaks due to the presence of the H_2 molecule. c) The projected DOS of the s-orbitals for Ti, H, and C, are shown together with the projected DOS of the carbon p-orbitals, $p_{x,y}$ and p_z. Details on the origin of the peaks labeled 1–4 are given in the text.

To elucidate the origin of the peak splitting in the density-of-states, the partial charge densities of the bands labeled 1 to 4 were calculated. **Figure** 6a,b show the partial charge densities that are attributed to the peaks located at $E_1 = -13.69$ eV and $E_2 = -12.50$ eV, respectively. For peak 1 the charge distribution extends from the C atoms over the H_2 molecule and exhibits a minor contribution from the central Ti atoms (Figure 6a). Peak 2 resides 1.19 eV higher in energy. It is characterized by the fact that the orbitals do not span the H–H bond (Figure 6b). Both charge densities reflect the s-like character of the bonding between the involved atoms.

For the energetically shallower peaks a similar behavior is observed. The partial charge density corresponding to peak 3 ($E_3 = -7.11$ eV) shows that the orbitals are extend along the H–H bond, while for the peak located at position 4 ($E_4 = -6.67$ eV) the charge

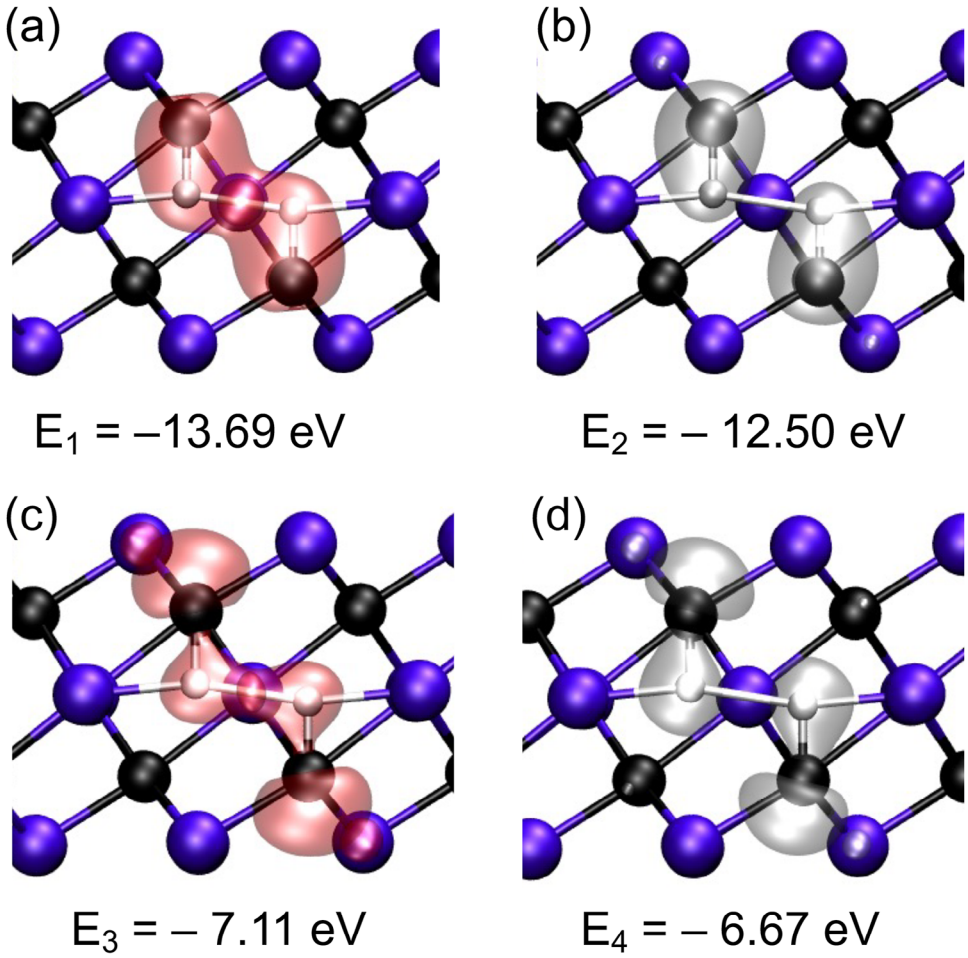

Figure 6. Atomic positions of H_2 in Ti_3C_2 together with the partial charge densities of the bands labeled 1 to 4 in Figure 5c. The energy values of the peaks in the DOS are indicated in (a–d). The value of the iso-surfaces amounts to 0.05 eVÅ^{-3}.

density does not extend along the H–H bond. A closer examination of the charge densities shows the typical dumbbell structure along the C–H bonds and the s-like orbital on the far side of the C atoms.

The final investigated position for H_2 molecules is the space between two Ti_3C_2 sheets. Interestingly, both H atoms move into equivalent positions next to each other (**Figure** 7a). However, this results in a distance of the two H atoms of 3.11 Å, which is beyond the distance where a stable bond will form. Hence, placing H_2 between Ti_3C_2 sheets results in a dissociation reaction. The presence of the two H atoms between the Ti_3C_2 sheets gives rise to two additional peaks in the total DOS at $E = -6.73$ and -6.30 eV (Figure 7b). Projection of the DOS on the H and nearest neighbor Ti atoms reveals that the peak located at $E = -6.73$ eV originates mainly from a superposition of the s-orbitals of nearest Ti atoms and the H atoms. One of the two nearest Ti atoms is indicated in Figure 7a. Note that the partial charge densities of both H atoms overlap at the nearest Ti atoms (Figure 7a). The second peak in the DOS originates mainly from the interaction of the s orbitals of the six outer Ti atoms with the H atoms (Figure 7c).

The stability of the hydrogen multicenter bonds was analyzed by calculating the formation energies. For this purpose the energy required to add an H atom or molecule from a reservoir into the solid was determined. For H atoms accommodated at the surface or between layers the formation energies amount to $E_f = -1.304$ and -0.87 eV, respectively. In case of H_2 molecules E_f decreases further to -2.035 and -1.585 eV. The formation energies for interstitial H and H_2 amount to 1.036 and 2.546 eV, respectively, which allows these complexes to be formed at moderate temperatures. The obtained values of formation energy are summarized in **Table** 1.

2.3. Vibrational Modes

For the six different configurations of monatomic and molecular H in Ti_3C_2 the vibrational frequencies and intensities for all $3N$ modes were calculated using density-functional perturbation theory (DFPT). The derived intensities were normalized to unity. A spectral distribution was calculated for each configuration by broadening the intensity eigenvalue data with a Gaussian resolution function with a width of 8 cm^{-1} and a scaled normalized intensity of 0.95. In (**Figure** 8a–c) the vibrational spectra for monatomic H on the surface, in the layer, and between two Ti_3C_2

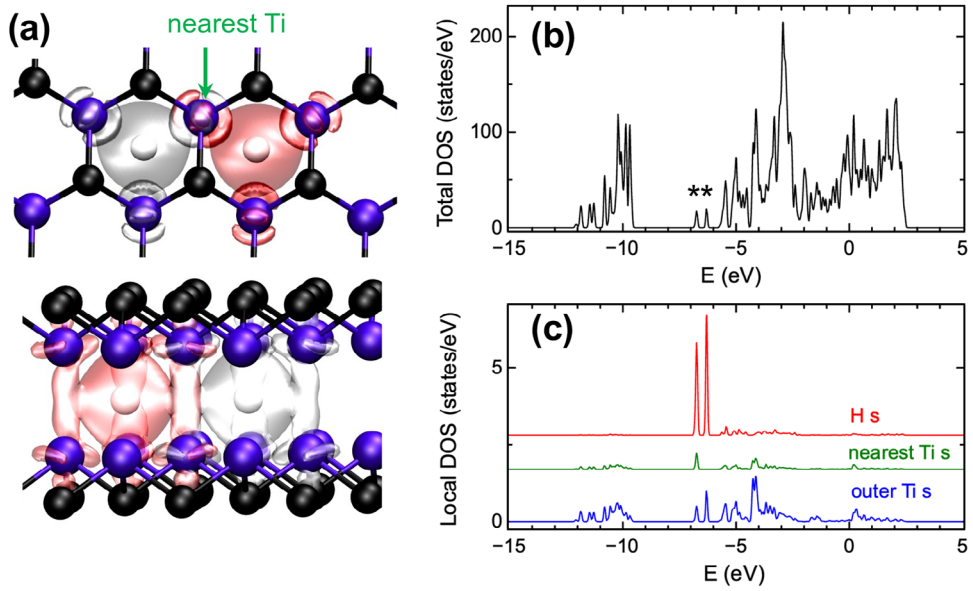

Figure 7. Depiction of the equilibrium positions of molecular hydrogen (H_2) between two Ti_3C_2 sheets. Shown are an edge-on and a top view projection a) including iso-surfaces corresponding to the lowest energy bonding state of the hydrogen molecule. To better distinguish between the two atoms the iso-surfaces are shown in different colors. The cutoff amounts to 8×10^{-3} eV Å^{-3}. b) The total density-of-states (DOS) is depicted. The asterisks mark the new peaks due to the presence of the H_2 molecule. c) Shows the projected DOS of the s-orbitals for Ti and H.

Table 1. Formation energies for monatomic and molecular hydrogen in Ti_3C_2.

	Surface	Interstitial	In between
E_f (H) (eV)	−1.304	1.036	−0.870
E_f (H_2) (eV)	−2.035	2.546	−1.585

sheets are shown, respectively. For H on the surface the largest amplitude is observed for the wagging modes at 953.1 and 955.5 cm^{-1}. This mode is degenerate. Most likely, the small difference in frequency is due to a numerical error. The contribution of the stretching vibrational mode at 934.6 cm^{-1} is negligible. The vibrational frequencies and the corresponding normalized intensities are summarized in **Table 2** for all configurations.

For interstitial hydrogen two peaks are observed at 1300.2 and 1551.9 cm^{-1} (Figure 8b). The vibrational mode located at 1300.1 cm^{-1} is attributed to a degenerate wagging mode while the dominant vibrational mode is attributed to a C–H stretching mode (see **Figure 9**).

When H atoms are accommodated between Ti_3C_2 sheets, three peaks are observable in the vibrational spectra at 992.9, 1106.6, and 1374.6 cm^{-1} (Figure 8c). The degeneracy of the first two modes is lifted because one of the three tetrahedral bond angles amounts to 126.3°, while the other two angles measure 109.6°. The third vibrational mode located at 1374.6 cm^{-1} corresponds to a stretching vibration of the H atom with respect to the Ti atom in the top Ti_3C_2 sheet (see Figure 9). Compared to H at the surface, its frequency is shifted to a larger value by 440 cm^{-1} indicating that this configuration is more stable.

For H_2 the number of vibrational modes doubles. The Gaussian broadened spectrum for H_2 adsorbed on the Ti_3C_2 surface exhibits 3 main peaks located at 287, 913, and 1147 cm^{-1} (Figure 8d). The corresponding eigenmodes are shown in the top row of (**Figure 10**). With respect to the outermost Ti along the H–H bond the modes are classified as follows. The vibrational modes at 287.3 and 906.7 cm^{-1} are H wagging modes. The lower frequency mode is attributed to the motion of the H atom that resides higher above the Ti_3C_2 surface. The vibrational modes located at 892.2 and 913.3 cm^{-1} are caused by an asymmetric and symmetric bending vibration, respectively. Finally, the modes located at 1147.1 and 1263.7 cm^{-1} are due to an asymmetric and symmetric stretching vibration, respectively (see Figure 10).

Interstitial H_2 shows only one relevant vibrational mode that is located at a wavenumber of 1431.9 cm^{-1} (Figure 8c). The intensities of the other 5 modes are zero (see Table 1). The prominent vibrational mode corresponds to an asymmetric stretching vibration of the two H atoms with respect to the neighboring Ti atoms in the direction of the H–H bond (see Figure 10).

When H_2 is introduced between two Ti_3C_2 sheets, the molecule dissociates and forms two hydrogen centers that are identical to monatomic H between two sheets of Ti_3C_2 (see Figures 3a and 7a). Consequently, the vibrational spectra are expected to be similar, which is indeed the case (see Figure 8c,f). Most likely, the small shift of the peaks to lower wave numbers for two H atoms is due to subtle structural variations caused by the proximity of the two H atoms. The vibrational modes located at 973.8, 977.6, 1035.9, and 1039.8 cm^{-1} correspond to symmetric and asymmetric wagging modes. Two groups of wagging modes are observed since the H atoms form asymmetric centers with the nearest neighbor Ti atoms. The symmetric wagging mode located at 1035.9 cm^{-1} shows the largest contribution to the vibrational spectrum. The local vibrational modes located at 1369.0 and 1372.3 cm^{-1} are attributed to the symmetric and asymmetric stretching mode of H with respect to the single Ti atom in the bottom Ti_3C_2 sheet (see Figure 10).

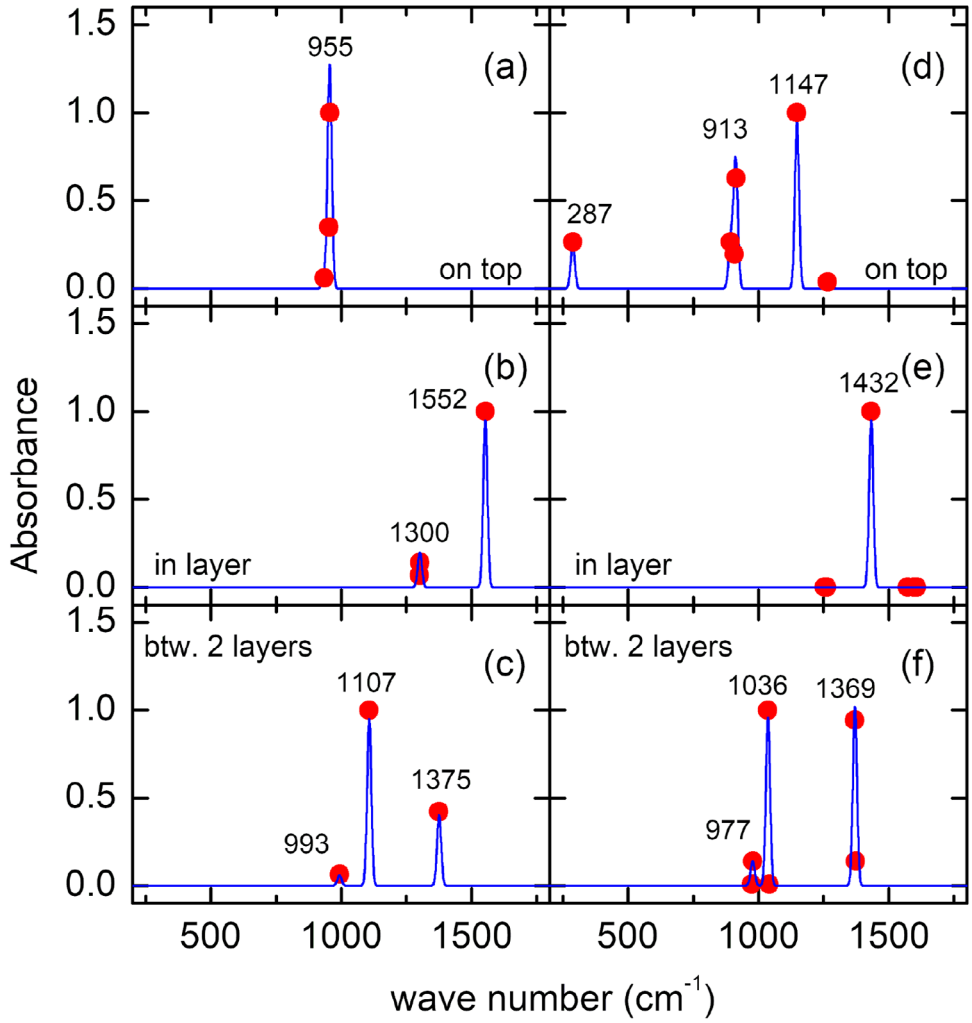

Figure 8. a–c) Calculated vibrational spectra of atomic (left column) and d–f) molecular hydrogen (right column) in Ti_3C_2. The data points represent the calculated frequencies and the solid lines represent Gaussian broadened spectra with a width of 8 cm^{-1}. The indicated frequencies correspond to the Gaussian broadened spectra. The exact frequencies of all modes are summarized in Table 2.

Table 2. Calculated vibrational properties for monatomic and molecular hydrogen in Ti_3C_2. The data were derived by employing density-functional perturbation theory. ω and A denote the vibrational frequency and amplitudes, respectively. The amplitudes are normalized to unity.

	Surface	H Interstitial	In between	Surface	H_2 Interstitial	In between
ω_1 [cm^{-1}]	934.6	1300.2	992.9	287.3	1252.2	973.8
A [a.u.]	0.06	0.07	0.06	0.26	0.0	0.01
ω_2 [cm^{-1}]	953.1	1301.1	1106.6	892.2	1260.4	977.6
A [a.u.]	0.35	0.14	1.0	0.26	0.0	0.14
ω_3 [cm^{-1}]	955.5	1551.9	1374.6	906.7	1431.9	1035.9
A [a.u.]	1.0	1.0	0.42	0.2	1.0	1.0
ω_4 [cm^{-1}]	...	...	...	913.3	1571.7	1039.8
A [a.u.]	...	...	...	0.63	0.0	0.01
ω_5 [cm^{-1}]	...	...	...	1147.1	1594.7	1369.0
A [a.u.]	...	...	...	1.0	0.0	0.94.
ω_6 [cm^{-1}]	...	...	...	1263.7	1607.1	1372.3
A [a.u.]	...	...	...	0.04	0.0	0.14

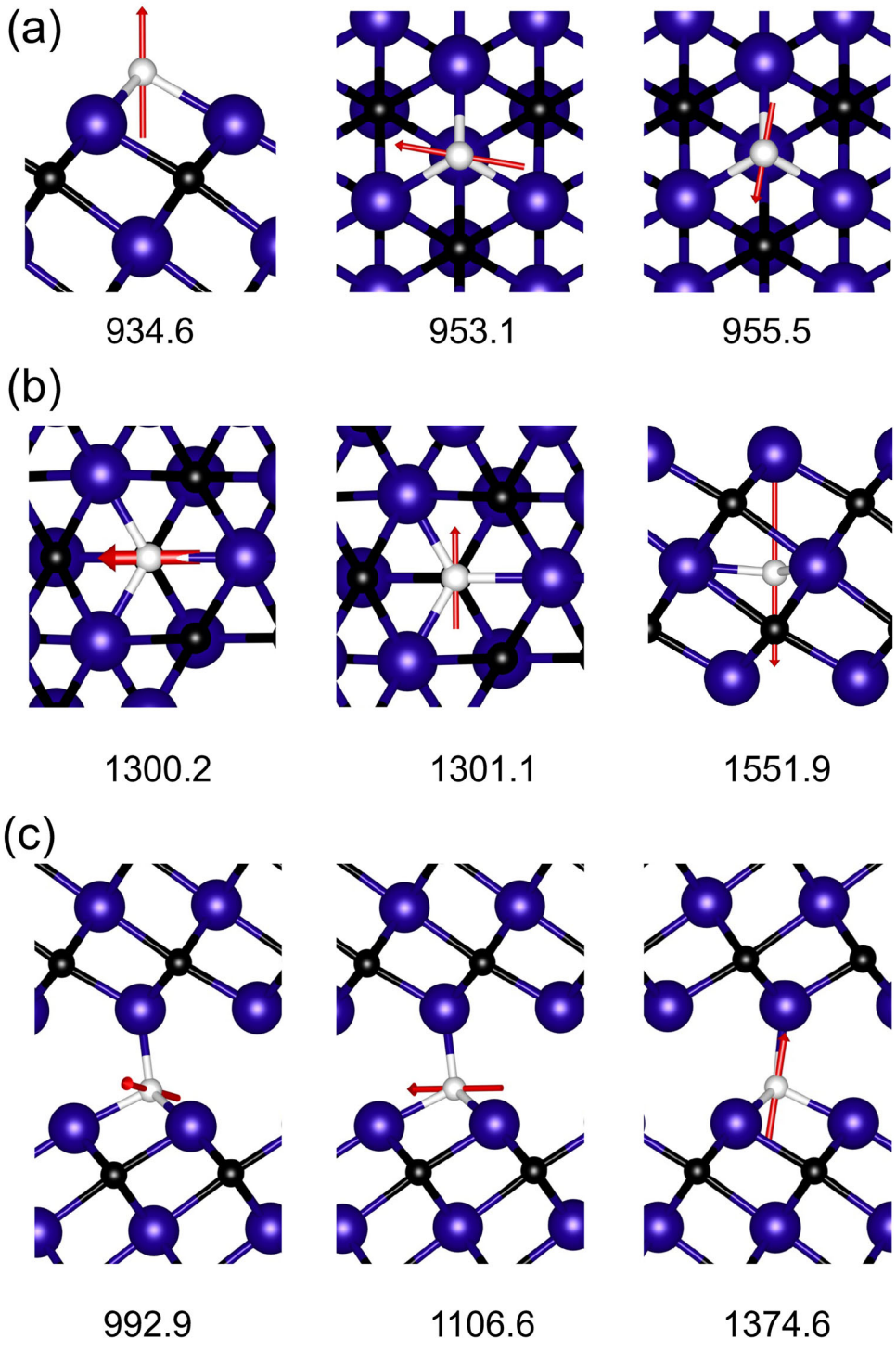

Figure 9. Eigenvectors of the vibrational eigenstates of atomic H for a) surface H, b) interstitial H, and c) H atoms between two Ti_3C_2 sheets. The numbers are the eigenfrequencies of the vibrational modes in cm^{-1}.

3. Summary

In summary,first-principles calculations based on density-functional theory were performed to investigate the interaction of H atoms and molecules with Ti_3C_2 MXenes. At the surface monatomic H assumes a stable position in a hexagonal center, which results in the formation of 3 Ti–H bonds. A similar stable position was found for H_2 molecules bonding with 6 nearest neighbor Ti atoms. Within MXene layers the interstitial site can accommodate H atoms and H_2 molecules. In addition

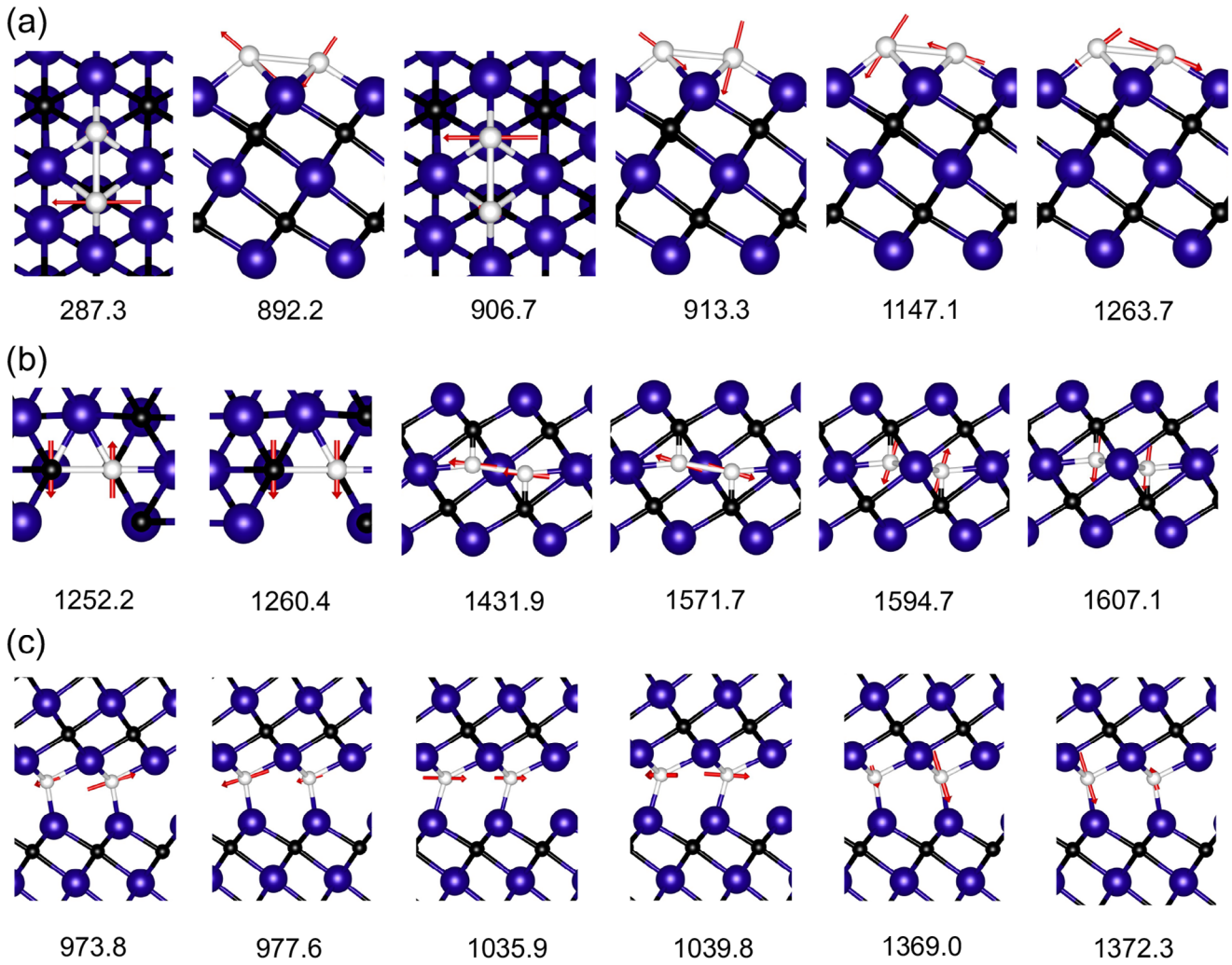

Figure 10. Eigenvectors of the vibrational eigenstates of molecular H a) on the surface of Ti_3C_2, b) at the interstitial site, and c) between two Ti_3C_2 sheets. The numbers are the eigenfrequencies of the vibrational modes in cm^{-1}.

to the formation of s-like bonds with neighboring Ti atoms, hydrogen also forms bonds with the nearest neighbor C atoms that are characterized by the formation of s–p hybrid orbitals. It is interesting to note that the H–H bond length is increased by a factor of 2.67 and 2.47 for H_2 on the surface and at the interstitial site, respectively. Hydrogen also tends to migrate into the space between two Ti_3C_2 sheets. The H atoms form three bonds with the surface Ti atoms of one Ti_3C_2 sheet and a fourth bond with a Ti surface atom of the second sheet. Interestingly, the H_2 molecule dissociates and forms two separate H-Ti_4 complexes. For all hydrogen configurations the vibrational frequencies and intensities were calculated using DFPT. All frequencies occur between 892 and 1607 cm^{-1} except for one bending vibration of H_2 at the surface of Ti_3C_2. The relatively high vibrational frequencies indicate that the H complexes are stable. The results show that the interaction of monatomic and molecular hydrogen with MXenes is beneficial from an energetic point of view. The observation that H_2 molecules between MXene sheets dissociate into monatomic H may potentially lead to enhanced in-diffusion. This effect may be beneficial for H storage applications. On the other hand, the interaction of H with MXenes may lead to material failure due to the formation of H-related complexes. Such a behavior is well-known in metals as hydrogen embrittlement.[24]

4. Computational Details

The calculations and the derived results were obtained from a first-principles approach based on DFT. Ti_3C_2 layers and surfaces were modeled in a slab geometry using hexagonal and rectangular supercells of 45 and 60 atoms, respectively. MXene double layers were modeled in hexagonal supercells with up to 90 atoms. The vacuum region amounted to 10.34 Å. The Vienna ab initio simulation package (VASP)[25,26] was used for the calculations using the generalized gradient approximation in the formulation of

Perdew, Burke, and Ernzerhof.[27] The s and d electrons of Ti were treated as valence electrons in the projector augmented wave method. For the calculations the local density approximation (LDA) + U was employed. U describes the onsite Coulomb interaction and amounts to 2.8 eV for titanium.[28] For the calculations a plane-wave cutoff of 700 eV was chosen. A Γ-centered k-point mesh of $3 \times 3 \times 1$ and $4 \times 4 \times 1$ was used for the large and small supercells, respectively. To obtain equilibrium structures ionic relaxation calculations were carried out until the forces acting on the atoms reached a value of 10^{-3} eV Å^{-1}. The Van der Waals interaction was not taken into account for these calculations, because its influence is negligible on the binding of hydrogen.

The properties of H and H_2 were further analyzed by calculating the vibrational eigenmodes and their intensities. For this purpose DFPT as implemented in VASP[25,26] was employed. This model provides a connection between the ground state electron density and the second derivative of the total energy and accounts for the linear response of the charge density to the displacement of the ions by an external applied field. The intensities of the infrared vibrational modes, A, are calculated from the Born effective charges, $Z^*_{a,b}$, and the eigenvectors $e_b(i)$ according to[29,30]

$$A = \sum_{a=1}^{3} \left(\sum_{i=1}^{N} \sum_{b=1}^{3} Z^*_{a,b} e_b(i) \right)^2 \quad (1)$$

Here, a and b denote the Cartesian polarizations and the number of atoms present is accounted for by the sum over i.

Acknowledgements

Open access funding enabled and organized by Projekt DEAL.

Conflict of Interest

The authors declare no conflict of interest.

Data Availability Statement

The data that support the findings of this article are available from the author upon reasonable request.

Keywords

hydrogen molecules and atoms, multicenter bonds, s-p hybridization, Ti_3C_2 MXenes

Received: January 22, 2024
Published online: February 22, 2024

[1] C. G. V. de Walle, P. J. H. Denteneer, Y. Bar-Yam, S. T. Pantelides, *Phys. Rev. B* **1989**, *39*, 10791.
[2] Y. V. Gorelkinskii, N. N. Nevinnyi, *Phys. B1* **1991**, *170*, 155.
[3] W. N. Lipscomb, *Boron Hydrides*, W. A. Benjamin Inc., New York **1963**.
[4] A. Janotti, C. G. Van De Walle, *Nat. Mater.* **2007**, *6*, 44.
[5] Y. Gogotsi, B. Anasori, *ACS Nano* **2019**, *13*, 8491.
[6] M. Naguib, O. Mashtalir, J. Carle, V. Presser, J. Lu, L. Hultman, Y. Gogotsi, M. W. Barsoum, *ACS Nano* **2012**, *6*, 1322.
[7] A. C. Rajan, A. Mishra, S. Satsangi, R. Vaish, H. Mizuseki, K. R. Lee, A. K. Singh, *Chem. Mater.* **2018**, *30*, 4031.
[8] R. Liu, W. Li, *ACS Omega* **2018**, *3*, 2609.
[9] Y. Wang, T. Guo, Z. Tian, K. Bibi, Y. Z. Zhang, H. N. Alshareef, *Adv. Mater.* **2022**, *34*, 2108560.
[10] B. Anasori, M. R. Lukatskaya, Y. Gogotsi, *Nat. Rev. Mater.* **2017**, *2*, 2.
[11] L. Cheng, X. Wang, F. Gong, T. Liu, Z. Liu, *Adv. Mater.* **2020**, *32*, 1902333.
[12] B. Anasori, Y. Gogotsi, *2D Metal Carbides and Nitrides (MXenes), Structure, Properties and Applications*, Springer, Berlin, Heidelberg **2019**.
[13] Z. Kang, M. A. Khan, Y. Gong, R. Javed, Y. Xu, D. Ye, H. Zhao, J. Zhang, *J. Mater. Chem. A* **2021**, *9*, 6089.
[14] S. Liu, J. Liu, X. Liu, J. Shang, L. Xu, R. Yu, J. Shui, *Nat. Nanotechnol.* **2021**, *16*, 331.
[15] N. C. Osti, M. Naguib, M. Tyagi, Y. Gogotsi, A. I. Kolesnikov, E. Mamontov, *Phys. Rev. Mater.* **2017**, *1*, 024004.
[16] Q. Hu, D. Sun, Q. Wu, H. Wang, L. Wang, B. Liu, A. Zhou, J. He, *J. Phys. Chem. A* **2013**, *117*, 14253.
[17] N. H. Nickel, W. B. Jackson, R. C. Bowman, R. G. Leisure, editors, *Hydrogen in Semiconductors and Metals: Vol. 513*, Materials Research Society, Warrendale, PA **1998**.
[18] J. I. Pankove, N. M. Johnson, *Hydrogen in Semiconductors*, Vol. *34*, Academic Press, San Diego, CA **1991**.
[19] N. H. Nickel, *Phys. Stat. Sol. (b)* **2023**, *260*, 2300309.
[20] Y. J. Chabal, *J. Mol. Struct.* **1993**, *292*, 65.
[21] S. Rivillon, Y. J. Chabal, F. Amy, A. Kahn, *Appl. Phys. Lett.* **2005**, *87*, 253101.
[22] B. N. Davidson, W. E. Pickett, *Phys. Rev. B* **1994**, *49*, 11253.
[23] D. Lide, *CRC Handbook of Chemistry and Physics*, 87th Edition, Taylor & Francis, Oxfordshire **2006**.
[24] X. Li, X. Ma, J. Zhang, E. Akiyama, Y. Wang, X. Song, *Acta Metall. Sin.* **2020**, *33*, 759.
[25] G. Kresse, J. Furthmüller, *Phys. Rev. B* **1996**, *54*, 11169.
[26] G. Kresse, J. Joubert, *Phys. Rev. B* **1999**, *59*, 1758.
[27] J. Perdew, K. Burke, M. Ernzerhof, *Phys. Rev. Lett.* **1996**, *77*, 3865.
[28] M. A. Gluba, N. H. Nickel, *Phys. Rev. B* **2013**, *87*, 085204.
[29] K. Esfarjani, Y. Hashi, *Phys. Rev. B - Condens. Matter Mater. Phys.* **1998**, *57*, 223.
[30] D. Karhánek, T. Bučko, J. Hafner, *J. Phys. Condens. Matter* **2010**, *22*, 265006.